PCCP

ROYAL SOCIETY OF CHEMISTRY

PAPER

View Article Online
View Journal | View Issue

Cite this: *Phys. Chem. Chem. Phys.*, 2024, **26**, 4492

Enhanced fluidity of water in superhydrophobic nanotubes: estimating viscosity using jump-corrected confined Stokes–Einstein approach†

Golam Rosul Khan and Snehasis Daschakraborty *

Received 4th December 2023,
Accepted 3rd January 2024

DOI: 10.1039/d3cp05906e

rsc.li/pccp

Accurately predicting the viscosity of water confined within nanotubes is vital for various technological applications. Traditional methods have failed in this regard, necessitating a novel approach. We introduced the jump-corrected confined Stokes–Einstein (JCSE) method and now employ the same to estimate the viscosity and diffusion in superhydrophobic nanotubes. Our study covers a temperature range of 230–300 K and considers three nanotube diameters. Results show that water inside superhydrophobic nanotubes exhibits a significantly lower viscosity and higher diffusion than those inside hydrophobic nanotubes. Narrower nanotubes and lower temperatures accentuate these effects. Furthermore, water inside superhydrophobic nanotubes display a lower viscosity than bulk water, with the difference increasing at lower temperatures. This reduction is attributed to weaker water–water interactions caused by a lower water density in the interfacial region. These findings highlight the importance of interfacial water density and its influence on nanotube viscosity, shedding light on nanoscale fluid dynamics and opening avenues for diverse applications.

1. Introduction

The behaviour of water inside nanochannels is pivotal in numerous technology applications, such as osmotic energy conversion,[1–4] biomedical diagnostics,[5] water purification,[6] desalination of water,[7–11] and energy storage.[12] The fluidity of water plays a major role in these applications. For example, an efficient desalination process or ultrahigh output power density from osmotic energy conversion can be only achieved with fast diffusivity of water through the nanochannels. Therefore, it is important to have a detailed understanding on the water dynamics inside nanotubes. Unfortunately, there is no general consensus about the actual impact of cylindrical nanochannels on the fluidity of water.[13–24] While one group of studies suggest an increase in the diffusivity of water due to confinement,[25,26] contradicting views also exist.[8,25,27] Actually, the effect of confinement on water fluidity is highly dependent on multiple factors, such as pore diameter, hydrophobicity of the channel material, density of the confined water, and temperature.

Although the diffusion of water inside nanochannels was reported in various experimental[15,17,18,20,21] and simulation[13,22–24,28] studies, the estimation of viscosity was rarely reported in the literature. This is because of the unavailability of a suitable experimental technique. The average viscosity of water in nanochannels is a fundamental parameter that plays a vital role in determining the performance of nanofluidic systems across a range of applications. It is essential for designing and optimizing nanoscale devices and processes in fields such as microfluidics, nanomedicine, materials science, and environmental sensing. Although the average viscosity does not directly regulate the local diffusion, that is the radial distribution of diffusivity, the overall diffusivity of water inside the nanochannel is of course regulated by the medium viscosity in the channel. The industrial application of water-filled nanotubes requires an estimate of the average diffusivity of water. Therefore, the calculation of average viscosity is crucial. The available theoretical methods were not free from issues. For example, studies using the Green–Kubo (GK) equation[29–32] reported unnaturally low viscosity (approximately 1/50th of the bulk water) of water in both hydrophobic and superhydrophobic

Department of Chemistry, Indian Institute of Technology Patna, Bihar 801106, India. E-mail: snehasis@iitp.ac.in

† Electronic supplementary information (ESI) available: The ESI includes the following eight sections. (S1) Method for estimation of the contact angle and characteristics snapshots of water droplet on the graphene sheet; (S2) Radial density profile of water inside the superhydrophobic carbon-nanotubes; (S3) 2D densmap profile of all systems at 230 K temperature; (S4) Mean square displacement (MSD) of water as functions of time for all systems; (S5) justification of the linear regime of the MSD plot; (S6) For all systems simulated and theoretical van Hove correlation functions plots; (S7) H-bond correlation function plots for overall systems; (S8) Table 1 for the viscosity values of water using Green–Kubo (GK) relation, confined-Stokes–Einstein (CSE), and the jump-corrected confined-Stokes–Einstein (JCSE) approaches; (S8) The amplitude and time scale of the hydrogen bond correlation functions for all systems represented in Table 2. See DOI: https://doi.org/10.1039/d3cp05906e

nanotubes.[22,33,34] This is probably due to the occurrence of highly unsymmetrical stress tensors in three directions. An alternative method, based on the confined Stokes–Einstein (CSE) relation,[22,35] was proposed. Unfortunately, the CSE relation assumed complete validity of the SE relation, which is less applicable in supercooled water,[36–41] pressurized superheated water,[42] water under confinement,[13,14,33] the presence of impurity (*e.g.*, solutes and other solvents),[43–46] *etc.* In our previous work,[34] we have proposed a novel approach, namely, the jump-corrected confined Stokes–Einstein (JCSE) relation, which takes into account both the system size effect and the breakdown of the SE relation to predict the viscosity of nanoconfined water. Note since the viscosity is a bulk quantity, we predict the micro-viscosity of water inside the nanoconfinement. The JCSE relation is based on the translational jump-diffusion (TJD) approach[34,36,37,45–51] that provides a quantitative explanation of the breakdown of the SE relation in supercooled water and aqueous solutions.

We computed the viscosity of water in three different hydrophobic nanotubes (CNT(n,n); with n = 10, 15, and 20) in a wide range of temperatures, including the supercooled regime.[34,37,49] Interestingly, the viscosity of water in narrow CNT(10,10) was observed to be surprisingly high compared to bulk water under the same thermodynamic condition.[33] The high viscosity of water inside nanochannels would forbid the use of the nanochannel in various applications, where high fluidity of water is desirable.[52,53] Since the confinement largely impacts the viscosity of water, the chemical nature of the channel wall (the extent of hydrophobicity) must influence the fluidity of water. Here, we are interested to know how superhydrophobic nanochannels influence water fluidity in comparison to hydrophobic nanochannels. A hydrophobic surface is one that repels water. This property is known as hydrophobicity. Hydrophobic surfaces are usually nonpolar and prefer other neutral molecules and nonpolar solvents. The contact angle of water on a hydrophobic surface is $145^\circ > \theta \geq 90^\circ$.[54]

Superhydrophobic surface has a highly water repellent property with the contact angle $\theta \geq 145^\circ$ and a very low contact angle hysteresis ($<5^\circ$).[54] Some plant leaves have superhydrophobic surface that assists in self-cleaning properties.[55,56] Superhydrophobic surfaces can be made by modifying the surface chemistry and constructing micro- or nanostructures on the surface.[57–63] The key to creating a superhydrophobic surface is to introduce a micro or nano-scale roughness to the surface,[64] which traps air pockets and prevents water from wetting the surface.[65] Designing a smooth superhydrophobic surface is a challenge. However, to solve the problem, we considered obtaining a smooth superhydrophobic surface by tuning the water-channel wall interaction. It is essential to ascertain whether a similar smooth surface can be employed for a superhydrophobic nanotube. To achieve this, we fine-tuned the cross-interaction parameter based on the contact angle formed by the water droplet on the surface. While it may not replicate an actual superhydrophobic surface, it has provided us with a model of a superhydrophobic surface.

The interior surface of CNTs is hydrophobic in nature with moderate water repellent property. The designing of superhydrophobic surface involves creation of micro-ruggedness on the surface followed by chemical surface changes to produce nanoscale ruggedness.[58,66–70] The superhydrophobic CNTs have a normally higher slip length than that of hydrophobic CNTs, and thus, more useful in the applications where higher fluidity of water is desirable.[52,53] In this regard, it is important to know how the superhydrophobicity of the channel wall affects the fluidity of water. However, to the best of our knowledge, no prior studies focused on this aspect. In the present work, we estimated the viscosity of water inside a model superhydrophobic nanochannel using the JCSE method. Three different superhydrophobic nanotubes (CNT (n,n); with n = 10, 15, and 20) are considered by varying the diameter between 1.36 nm and 2.60 nm. We have compared our results for the superhydrophobic nanotubes with those for the hydrophobic nanotubes and bulk water and provided possible explanations of the findings.

2. Methodology

2.1. Simulation details

First, we simulated bulk water and then water inside the three armchair superhydrophobic CNTs (n,n); n = 10 (diameter d = 1.36 nm), 15 (diameter d = 2.03 nm), and 20 (diameter d = 2.60 nm) each at eight different temperatures: T = 230, 240, 250, 260, 270, 280, 290, and 300 K. We have considered 10 nm length for the CNTs and packed water maintaining the effective density of ρ_{eff} = 1.0 g cm^{-3}.[34,71] The following equation is used to determine ρ_{eff} as follows:[34]

$$\rho_{\text{eff}} = \frac{m}{\pi L_{\text{CNT}} (d_{\text{eff}}/2)^2} \quad (1)$$

In the above equation, $d_{\text{eff}} = d - \sigma_{\text{co}}$, where σ_{co} is the LJ diameter associated with the interaction between water O and C of the CNT. A few earlier studies indicated the occurrence of less water density inside CNTs compared to bulk.[27,72,73] However, since this work is mainly focused on a comparative study between the viscosity of water inside a superhydrophobic nanotube and a hydrophobic nanotube, we keep the water density constant, so that the effect of nanotube surface is clearly demonstrated. Fig. 1b and c present the nanotubes filled with water.

The CNTs are modelled with OPLS/AA force-field[74] where the constituent atoms are considered Lennard-Jones (LJ) particles with the force-field (σ_{cc} = 0.355 nm and ε_{CC} = 0.2929 kJ mol^{-1}).[22,34] The water molecules are modelled using the TIP4P/2005 force-field.[75] The interaction between the C atoms of CNTs and the water O atoms is described by LJ interaction parameters: σ_{co} = 0.3349 nm and ε_{CO} = 0.047 kJ mol^{-1}.[22] The force-field parameters used in our previous work[34] for hydrophobic carbon nanotubes (CNTs) are similar to the above-mentioned values. However, for the hydrophobic CNT, a higher value of ε_{CO} (0.247 kJ mol^{-1})[22] was used. These force-field parameters are commonly employed for simulating water in superhydrophobic CNTs and water on graphene surfaces.[26,33,76,77] To further demonstrate this, we conducted simulations of a water nanodroplet on a

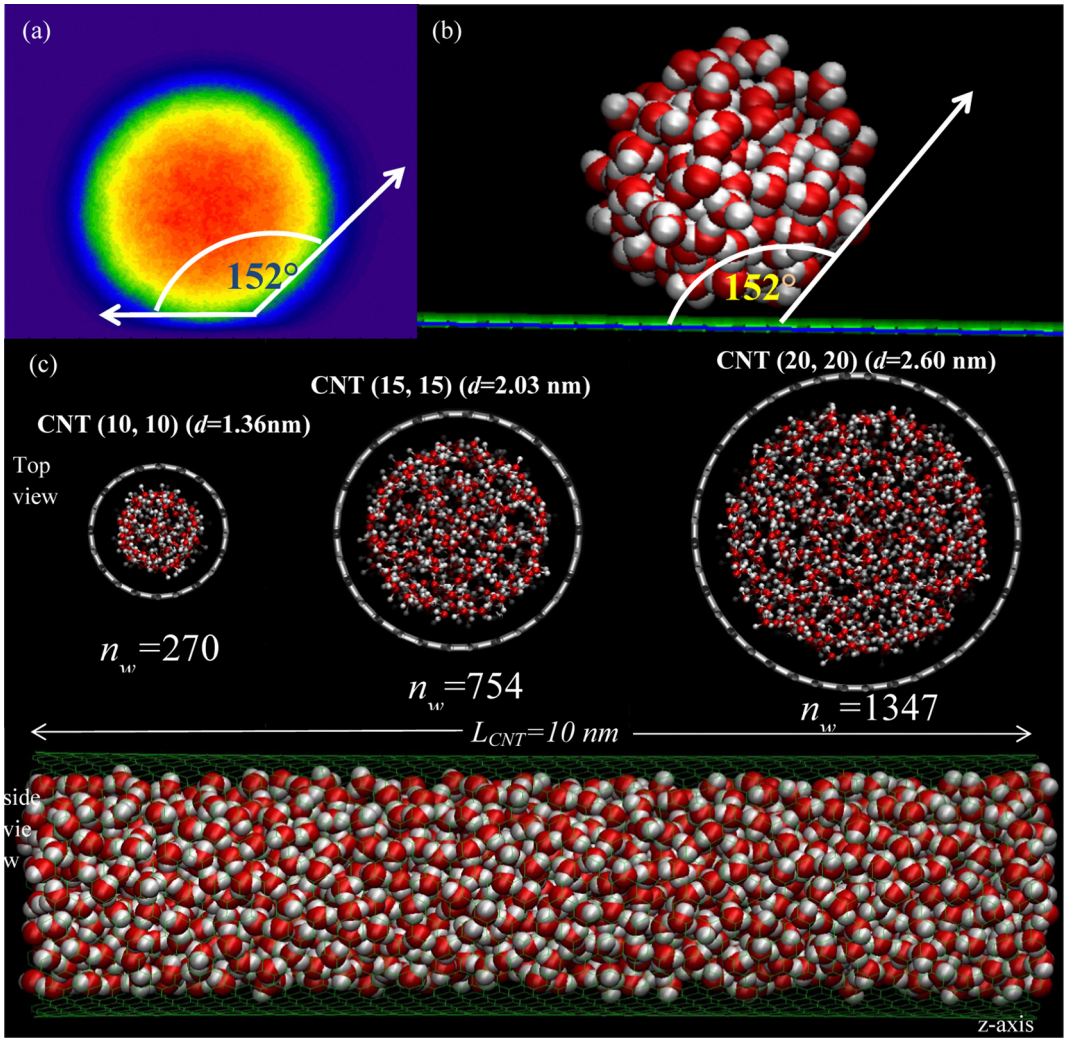

Fig. 1 (a) Two-dimensional density profiles of water nanodroplets (projected in the *yz* plane) on a graphene surface where the contact angle is mentioned. (b) Simulation snapshot for the water nanodroplet on a superhydrophobic surface. Following are the colour codes used in panel (b): green for the surface atoms, red colour for the water oxygen atoms and white for hydrogen atoms. (c) Snapshots represent the top and side views of the water filled nanotube systems.

graphene surface using the same force-field parameters described earlier. The contact angle was estimated using the method[78] presented in Section S1 of the ESI.† In Fig. 1a, a snapshot of the water nano droplet on a superhydrophobic graphene surface is depicted, with the average contact angle estimated to be θ = 152°. This contact angle confirms the superhydrophobic nature of the graphene-like surface and the considered CNTs.

In the present simulation work, we conducted two sets of runs depending on the temperature range. For temperatures below or equal to 270 K, the simulations are performed for a duration of 300 ns. For temperatures above 270 K, the simulations are run for 200 ns. In both cases, the initial 20 ns of the trajectory were excluded from the analysis. The simulations are run using the NVT ensemble, where the temperature is restricted using the Nośe–Hoover thermostat.[79,80] The simulation time step is chosen as 2 fs. Vacuum is created along *x* and *y* axes to avoid interactions between the periodic images in these directions. The box dimension is chosen as ($x \times y \times z$ = 5 nm × 5 nm × 10 nm). Periodic boundary conditions are applied in all three directions. The Verlet leapfrog algorithm is used for solving the equations of motion at every 2 fs. Long-range electrostatic interactions are solved by the particle mesh Ewald summation method.

2.2. Jump-corrected confined Stokes–Einstein (JCSE) approach

The JCSE approach for estimating the viscosity of water inside CNTs was detailed in our previous article.[34] Here, we summarize the method with the key equations involved. The JCSE equation for the viscosity of water confined in nanochannel η_{JCSE} can be written as follows:[34]

$$\eta_{\mathrm{JCSE}} = \frac{k_{\mathrm{B}}T}{3\pi\sigma_{\mathrm{h_{Res}}}D_{\mathrm{Res}_z}}\left[1+\frac{3}{8}\frac{\sigma_{\mathrm{h_{Res}}}}{d}\ln\left(\frac{2d}{\sigma_{\mathrm{h_{Res}}}}\right)\right] \qquad (2)$$

where k_{B} is the Boltzmann constant, T is the temperature, and d is the diameter of the CNT. D_{Res_z} is the residual diffusion coefficient along the *z*-axis. The hydrodynamic diameter

$\sigma_{h_{Res}}$ can be calculated from bulk water using the following equation:[34]

$$\sigma_{h_{Res}} = \frac{k_B T}{3\pi\eta_{bulk} D_{Res_{z_{bulk}}}} \quad (3)$$

In eqn (3), η_{bulk} is the viscosity and $D_{Res_{z_{bulk}}}$ is the residual diffusion coefficient for bulk water at temperature T. Eqn (2) is written from the confined Stokes–Einstein (CSE) equation[22,34] for the diffusion of water along the z-axis of the CNT. The CSE equation can be written as follows:[22,34]

$$\eta_{CSE} = \frac{k_B T}{3\pi\sigma_h D_z}\left[1 + \frac{3}{8}\frac{\sigma_h}{d}\ln\left(\frac{2d}{\sigma_h}\right)\right] \quad (4)$$

The derivation of eqn (4) is presented elsewhere.[22] Note that the main difference between the JCSE (eqn (2)) and CSE (eqn (4)) approaches is that in the JCSE equation, the residual diffusion coefficient D_{Res_z} replaces the total diffusion D_z in the CSE equation. Accordingly, the hydrodynamic diameter $\sigma_{h_{Res}}$ in the JCSE equation (eqn (2)) is calculated from the residual diffusion $D_{Res_{z_{bulk}}}$ of bulk water molecules.

Now we discuss about the residual diffusion coefficient D_{Res_z}: the method of calculation and its physical significance. The residual diffusion coefficient along the z-axis D_{Res_z} can be calculated using the translational jump-diffusion (TJD) approach.[34,36,37,46,48–50] Herein, we give a brief overview of the steps involved in the calculation of the residual diffusion coefficient D_{Res_z} of water molecules along the z-axis. First, the trajectories of each of the water molecules (t_{traj} duration) along the z-axis are divided into smaller fragments of duration t^*, which is the location of the maximum of non-Gaussian parameter $\alpha_2(t)$. For the dynamics along the z-axis, $\alpha_2(t)$ can be calculated using the following equation:[34,81]

$$\alpha_2(t) = \frac{\langle z^4(t)\rangle}{3\langle z^2(t)^2\rangle} - 1 \quad (5)$$

where $\langle z^4(t)\rangle = \langle[z(t+t_0) - z(t_0)]^4\rangle$ and $\langle z^2(t)\rangle = \langle[z(t+t_0) - z(t_0)]^2\rangle$. Here, $z(t_0)$ and $z(t+t_0)$ are the positions of a water molecule at times t_0 and $(t+t_0)$, respectively. The center of mass displacement of a molecule during a specific trajectory segment is determined using the following equation:[34,36,37,45–50]

$$\lambda_{z_i} = 2R_{z_{g,i}} = 2 \times \sqrt{\frac{1}{n}\sum_{(i-1)t^* \le t \le it^*}\left[z(t) - z_{CM,i}\right]^2} \quad (6)$$

In the above equation, $R_{z_{g,i}}$ is the radius of gyration of the ith trajectory segment, which is one of the total M ($M = t_{traj}/t^*$) number of smaller trajectory segments, $z(t)$ is the molecule's z-position at time t, and $z_{CM,i}$ is the center-of-mass of the ith trajectory segment, $z_{CM,i} = \frac{1}{n}\sum_{(i-1)t^* \le t \le it^*} z(t)$.

The determination of a minimum distance criterion for the translational jump involves comparing the self-part of the van Hove correlation function, denoted as $G_S^{simu}(z,t^*)$, at a specific time point t^* (the time when $\alpha_2(t)$ reaches its maximum) with the corresponding theoretical Gaussian distribution, represented by $G_S^{theo}(z,t^*)$. The calculations for $G_S^{simu}(z,t^*)$ and $G_S^{theo}(z,t^*)$ can be performed using the following equations:[46,49,82,83]

$$G_S^{simu}(z,t^*) = \langle\delta(z - [z(t_0) - z(t_0 + t^*)])\rangle \quad (7)$$

$$\left(G_S^{theo}(z,t^*)\right) = \left[\frac{1}{2\pi(MSD)_{at\ t=t^*}}\right]^{1/2}\exp\left[-\frac{z^2}{2(MSD)_{at\ t=t^*}}\right] \quad (8)$$

where the mean square displacement MSD can be calculated using the following equation:

$$MSD = \langle z^2(t)\rangle = \langle[z(t+t_0) - z(t_0)]^2\rangle \quad (9)$$

$G_S^{simu}(z,t^*)$ intersects with $G_S^{theo}(z,t^*)$ at two points. Beyond the second crossing point, denoted as z_2, the likelihood of experiencing larger displacements becomes higher than what is predicted by the Gaussian distribution. Consequently, we classify translational movements with $\lambda_{z_i} > z_2$ as translational jumps. By identifying these jumps, we can calculate the jump-diffusion coefficient D_{Jump_z} using the following equation:[34,45,47,48,50]

$$D_{Jump_z} = \frac{1}{2}\nu_{Jump_z}\lambda_{Jump_z}{}^2 \quad (10)$$

The jump frequency ν_{Jump_z} and the average square jump length $\lambda_{Jump_z}{}^2$ are calculated using the following equations:

$$\nu_{Jump_z} = \frac{N_{Jump_z}}{N\, t_{traj}} \quad (11)$$

$$\lambda_{Jump_z}{}^2 = \lim_{N_{Jump}\to\infty}\frac{1}{N_{Jump}}\sum_{j=1}^{N_{Jump}}\lambda_{j_z}{}^2 \quad (12)$$

The jump-diffusion coefficient D_{Jump_z} captures the diffusion resulting from these translational jumps along the z-axis. However, there are also "non-jumping" trajectory segments that contribute to a different diffusion behaviour characterized by small-step diffusion of water molecules.[34,45,49] This diffusion coefficient is referred to as the residual-diffusion coefficient, denoted by D_{Res_z}. It quantifies the diffusion associated with these small steps.[34,36,37,46,48]

$$D_{Res_z} = D_z - D_{Jump_z} \quad (13)$$

The physical significance of the residual diffusion lies in its ability to quantify one component of self-diffusion coefficient that originated from small-step displacement of the molecules following the Brownian motion.[36,37,84–87] Since the long-step translational jumps do not contribute to the residual diffusion, the latter is coupled to the viscosity of the medium fairly strongly irrespective of temperature and pressure variation or the presence of other water miscible solvents such as methanol and ethanol.[46,87,88] Eqn (13) was validated earlier[37] by evaluating D_{Jump} and D_{Res} independently using the MSD route. For this, the full trajectories were separated into two parts: the trajectory portion of the molecules containing only the jump events and the left over portion of the trajectory containing only small-step displacements. It was observed that the above-mentioned diffusion components, obtained from the MSD

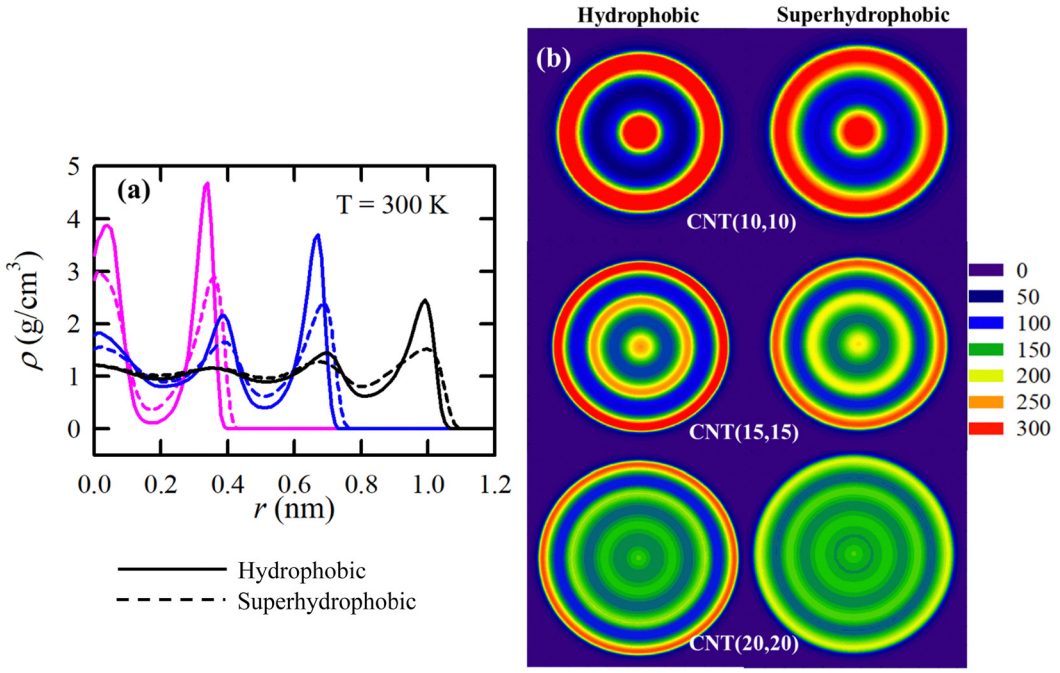

Fig. 2 (a) Radial density profiles of water inside hydrophobic and superhydrophobic CNTs at 300 K temperature for CNT(10,10) (pink), CNT(15,15) (blue), and CNT(20,20) (black). (b) Two-dimensional density maps, projected on the *xy* plane, of water in hydrophobic (left) and superhydrophobic (right) nanotubes at 300 K. The data for hydrophobic CNTs are taken from our previous work.[34]

route, are in close agreement with the values obtained using eqn (10)–(13). This validated the eqn (10)–(13).

3. Results and discussion

3.1. Radial density profile

Fig. 2a exhibits the density profiles of water inside three superhydrophobic nanotubes at a temperature of 300 K and compares with the results for hydrophobic nanotubes. (Fig. S2 of the ESI,† illustrates the density profiles for the remaining temperatures of water inside the superhydrophobic nanotubes.) The oscillating pattern of density profile manifests the layering of water molecules inside the nanotubes. There are two discernible layers of water in CNT(10,10), but the density does not reach the bulk value in the core region. For CNT(15,15) and CNT(20,20), three and four peaks are visible, respectively. The bulk density is attained in the core region only for CNT(20,20). By comparing the density profiles of water in hydrophobic and superhydrophobic CNTs, it is evident that the hydrophobicity of the wall strongly influences the intensity of the first peak. Around 40% lower first peak intensity was observed for superhydrophobic CNTs compared to hydrophobic ones, while around 20% less second peak height was observed in case of superhydrophobic CNTs compared to hydrophobic ones. Fig. S2 of the ESI,† shows weak temperature dependence of the radial density profile. These are consistent with earlier reports.[23]

The lower density peak intensities in case of superhydrophobic CNTs indicate more diffused water density in the superhydrophobic CNT. This is more evident in the two-dimensional density maps of water (averaged over *z*-axis) in hydrophobic and superhydrophobic nanotubes, as presented in Fig. 2b for 300 K (the density maps for 230 K are presented in Fig. S3 of the ESI†). Distinct spatial heterogeneity, resolved radially, is clearly visible in all three CNTs.

3.2. Diffusion

Now, we calculated the diffusion coefficient of water molecules along the *z*-axis. The mean square displacement (MSD) route is now used to calculate the diffusion of water molecules through CNTs in one dimension. The following equation is used to compute the MSD along the *z*-axis:[34]

$$\mathrm{MSD} = \langle |z(t) - z(0)|^2 \rangle \quad (14)$$

Here, $z(t)$ and $z(0)$ are the *z*-positions of a water molecule at time t and time $t = 0$. Fig. S4 of the ESI,† presents the MSD plots for the water molecules at different temperatures for bulk water and water inside three superhydrophobic CNTs. The diffusion coefficient of bulk water at room temperature is compared with that reported in the literature in Table S3 of the ESI,† where a good agreement is observed. The MSDs contain three contiguous regions: ballistic ($\langle |r(t)|^2 \rangle \propto t^2$) at beginning time, sub-diffusive ($\langle |r(t)|^2 \rangle \propto t^\gamma$; $0 < \gamma < 1$) at intermediate time, and diffusive ($\langle |\Delta r(t)|^2 \rangle \propto t$) at long time.[34,45,48] In Fig. S5 (ESI†), we depict the variation in γ over time for the different systems. It is evident that $\gamma(t)$ reaches its minimum at an intermediate time of approximately 1 ps. As the temperature decreases, the minimum value of $\gamma(t)$ diminishes. For instance, in the case of CNT(10,10), the minimum value of $\gamma(t)$ decreases from around 0.65 to approximately 0.20 as the temperature decreases from 300 K to 230 K. This observation suggests that sub-diffusion

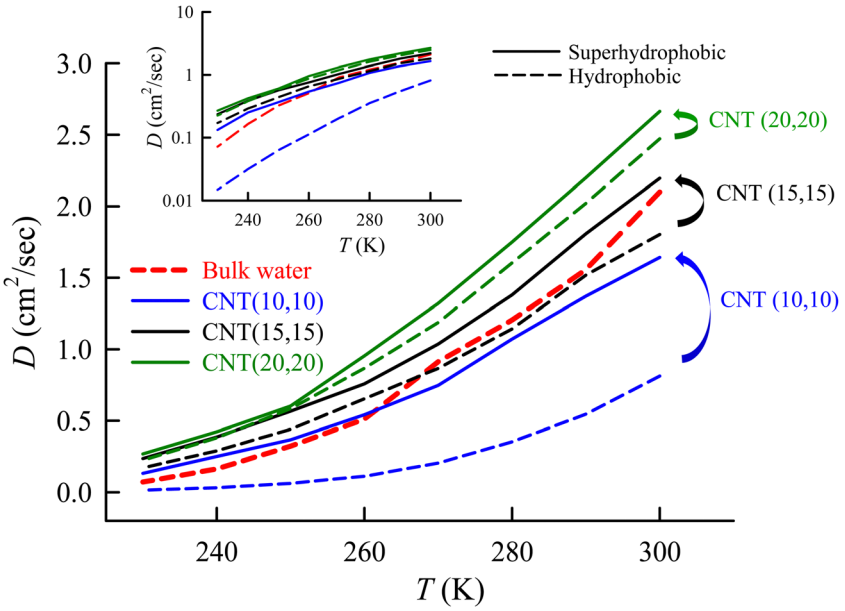

Fig. 3 Diffusion coefficient of water along the z-axis of superhydrophobic and hydrophobic CNTs and bulk water. The data for hydrophobic CNTs and bulk water are taken from our previous work.[34] The inset presents the data in the log-scale of diffusion axis.

becomes more pronounced at lower temperatures. Additionally, the degree of confinement also impacts the minimum value of $\gamma(t)$. For a given temperature, the most significant reduction in $\gamma(t)$ at intermediate time intervals is observed for CNT(10,10). Intriguingly, the $\gamma(t)$ minima values for water diffusion inside CNT(15,15) and CNT(20,20) exceed those observed in bulk water. This implies that confinement within these two nanotubes induces less trapping of water molecules compared to bulk water.

Now, we calculate the diffusion coefficient of water along the z-axis by fitting MSD with Einstein's equation beyond time when $\gamma(t)$ reaches unity:[34]

$$\text{MSD} = \langle |z(t) - z(0)|^2 \rangle = 2Dt \qquad (15)$$

Fig. 3 presents the diffusion coefficients of water as a function of temperature for three types of carbon nanotubes (CNTs): superhydrophobic CNTs, hydrophobic CNTs, and bulk water. The corresponding diffusivity values can be found in Table 1. The findings reveal a noticeable increase in water diffusivity within superhydrophobic CNTs compared to those in the other two types of CNTs and at various temperatures. The most significant enhancement is observed in CNT(10,10). For instance, at 300 K, water diffuses approximately twice as fast within superhydrophobic CNT(10,10) compared to that within hydrophobic CNT(10,10) at the same temperature, showing an increase of approximately 1.3 times and 1.1 times for CNT(15,15) and CNT(20,20), respectively. The disparity between hydrophobic and superhydrophobic CNTs becomes more pronounced at lower temperatures, particularly evident for CNT(10,10), as indicated in the inset of Fig. 3. At 230 K, the diffusivity of water within superhydrophobic CNT(10,10) is approximately 16 times higher than that within hydrophobic CNT(10,10). Unlike hydrophobic CNTs, the diffusion of water within superhydrophobic CNT(10,10) is only slightly lower than that of bulk water at 300 K. However, at lower temperatures, the diffusivity of water inside superhydrophobic CNTs surpasses that of bulk water. For example, at 230 K, water diffuses almost two times faster within superhydrophobic CNT(10,10) than bulk water, while the diffusion of water within superhydrophobic CNT(15,15) and CNT(20,20) is approximately 3 and 4 times faster respectively, than that of bulk water. The enhancement of diffusion inside the CNTs with a larger diameter was already reported in the literature.[25,26] The remarkable enhancement of water diffusivity within superhydrophobic CNT(10,10) in comparison to that within hydrophobic CNT(10,10) underscores the significant potential applications of superhydrophobic nanotubes.

Table 1 Diffusion coefficient of water inside different hydrophobic (hp) and superhydrophobic (shp) CNTs and bulk water at different temperatures. The data for hydrophobic CNTs and bulk water are taken from our previous work[34]

	$D/10^{-5}$ (cm^2 s^{-1})						
		CNT(10,10)		CNT(15,15)		CNT(20,20)	
T (K)	Bulk water	hp	shp	hp	shp	hp	shp
300	2.10	0.81	1.65	1.80	2.22	2.47	2.66
290	1.56	0.55	1.36	1.52	1.79	2.02	2.13
280	1.20	0.35	1.06	1.14	1.42	1.60	1.68
270	0.91	0.20	0.81	0.87	1.09	1.19	1.29
260	0.51	0.11	0.60	0.65	0.81	0.87	0.95
250	0.32	0.06	0.41	0.44	0.57	0.58	0.65
240	0.16	0.03	0.26	0.29	0.38	0.38	0.43
230	0.07	0.01	0.16	0.17	0.23	0.22	0.26

3.3. Estimation of viscosity through the JCSE approach

Now, we calculate the viscosity of water inside superhydrophobic CNTs using the JCSE approach, as detailed in Section 2.2.

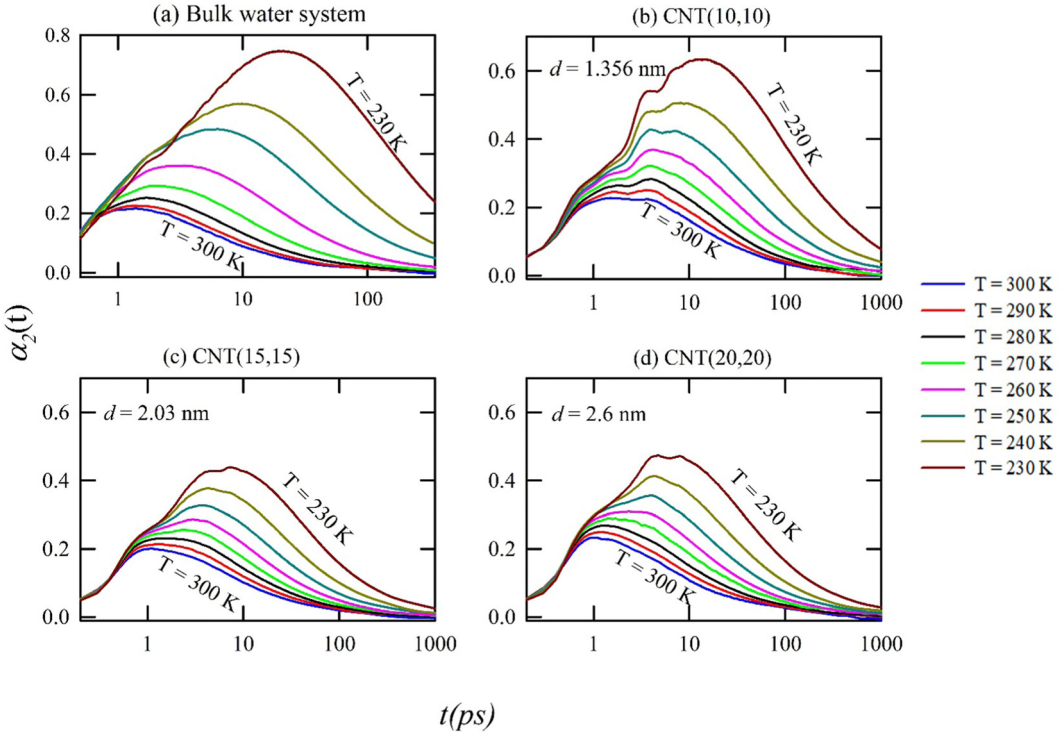

Fig. 4 Non-Gaussian parameter $\alpha_2(t)$ as a function of time at different temperatures for bulk water (a) and water in CNT(10,10) (b), CNT(15,15) (c), and CNT(20,20) (d) superhydrophobic nanotube systems.

For this we need to calculate the residual diffusion along the z-axis, D_{Res_z} through the TJD model.[34,36,37,46,49,50] We analyze the trajectory segments of time period t^*, and the peak position of the non-Gaussian parameter $\alpha_2(t)$ (eqn (5)). Fig. 4 presents the time-dependent $\alpha_2(t)$ for different temperatures for three superhydrophobic CNTs and bulk water. An increase by one order of magnitude is observed in the value of t^* for all the systems including bulk water with the reduction in temperature from 300 to 230 K. A higher peak height of $\alpha_2(t)$ at a lower temperature indicates larger dynamic heterogeneity.[34,45,87]

The net spatial movement of the water molecules λ_{z_i} during each trajectory segment of duration t^* was calculated using eqn (6). Now, the jump distance criteria need to be established from the van Hove correlation function. The self-part of the van Hove correlation function $G_S^{\mathrm{simu}}(z,t^*)$ is plotted as a function of z at time t^* and the same is compared with the theoretical Gaussian equation.[49] $G_S^{\mathrm{theo}}(z,t^*)$ in Fig. 5a and b represents the comparison of these two functions at 300 and 230 K, respectively. (The results at the remaining temperatures are exhibited in Fig. S6 of the ESI†) The non-Gaussian distribution is clearly visible in the long distance region beyond a distance r_2, the minimum cut-off for the jump-distance. Fig. 5c presents the minimum cut-off distance r_2 as a function of temperature for different superhydrophobic CNT systems and bulk water. As the jump-diffusion criterion is established, we calculated the jump-diffusion coefficient along the z-axis D_{Jump_z} using eqn (10), and the results are listed in Table 2. The jump-frequency ν_{Jump_z} and average square jump-length $\lambda_{\mathrm{Jump}_z}{}^2$ for different systems and temperatures are also listed in the same table.

Clearly, there are strong influences of temperature and confinement on both the parameters, ν_{Jump_z} and $\lambda_{\mathrm{Jump}_z}{}^2$. However, the jump-diffusion coefficient is less influenced by temperature compared to the total diffusion coefficient in all the cases. For example, D_{Jump_z} decreases from 4.56×10^{-7} cm^2 s^{-1} at 300 K to 2.18×10^{-7} cm^2 s^{-1} ($\sim$2 times) at 230 K for superhydrophobic CNT(10,10), while due to the same reduction in temperature, the total diffusion D_z decreases from 1.65×10^{-5} cm^2 s^{-1} to 0.16×10^{-5} cm^2 s^{-1} ($\sim$10 times). Therefore, the percentage contribution of the jump-diffusion, denoted by χ_{Jump} ($=100 \times D_{\mathrm{Jump}_z}/D_z$)[34,36,37,46,48–50] should increase with the decrease in temperature. This is, indeed, observed for all the systems with the decrease in temperature, as shown in Table 2. More interestingly, at a given temperature, χ_{Jump} for water inside superhydrophobic CNTs is less than that of bulk water. This indicates that the water molecules take a larger number of small steps while diffusing through superhydrophobic CNTs compared to that in bulk water. On comparing between hydrophobic and superhydrophobic CNTs (Fig. 5d), it is observed that the values of χ_{Jump} are overall owner for the superhydrophobic nanotubes compared to those in the hydrophobic CNTs, with the maximum deviation observed for superhydrophobic CNT(10,10) system. This means that inside the superhydrophobic CNT, the water molecules translate more *via* small steps instead of long steps compared to those inside the hydrophobic CNT.

Now, the residual diffusion coefficient D_{Res_z} was calculated by subtracting the jump-diffusion from the total diffusion D_z using eqn (13), and the values are listed in Table 1 for bulk

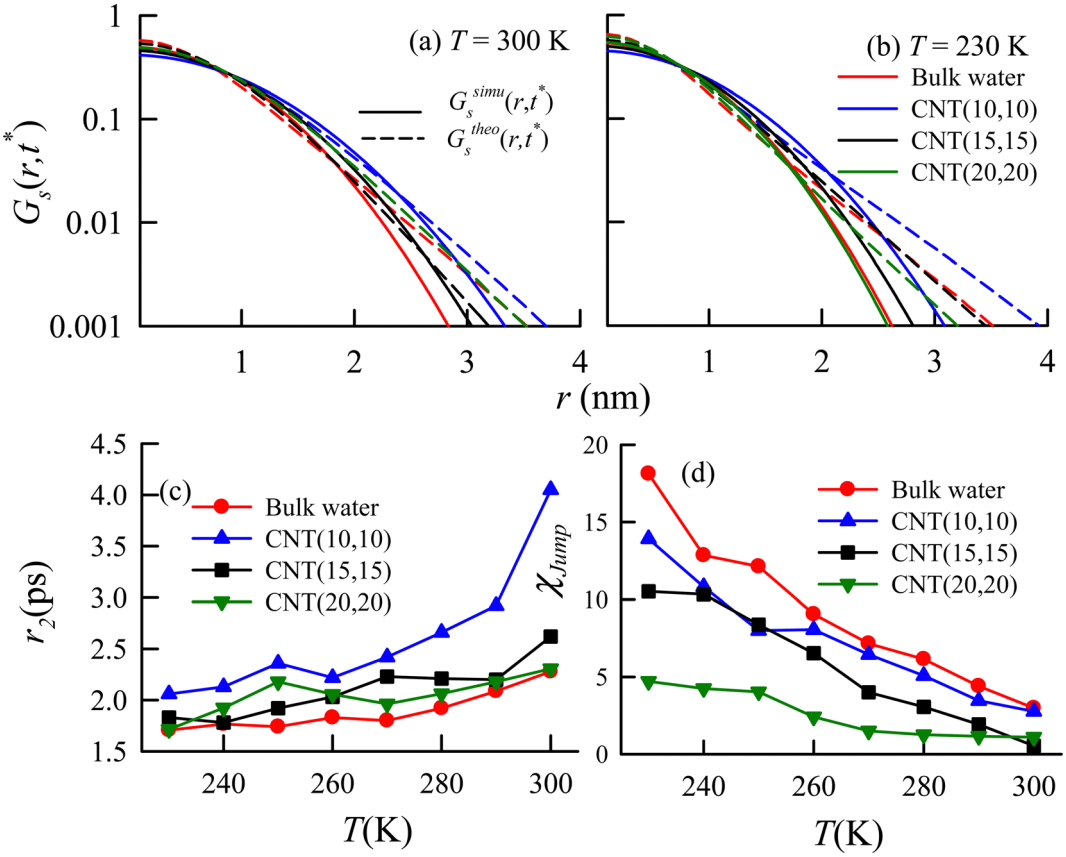

Fig. 5 Comparison between simulated $G_S^{simu}(z,t^*)$ (solid line) and theoretical van Hove correlation functions ($G_S^{theo}(z,t^*)$) (dashed line) at time t^* at 300 K (a) and 230 K (b) for water inside the CNT(10,10) (blue), CNT(15,15) (black), and CNT(20,20) (dark green) superhydrophobic nanotube systems. (c) Second crossing r_2 between $G_S^{simu}(z,t^*)$ and $G_S^{theo}(z,t^*)$, the minimum distance criteria for a jump occurrence. (d) Percentage contribution of the jump-diffusion for bulk water and water inside superhydrophobic CNTs.

water and water inside CNTs at different temperatures. The *residual* hydrodynamic diameter $\sigma_{h_{Res}}$ was calculated for bulk water using eqn (3), and the viscosity of the bulk water, η_{bulk}, presented in Table 2 for different temperatures, was calculated using the Green–Kubo relation. Finally, the numerical values of D_{Res_z} and $\sigma_{h_{Res}}$ are entered in eqn (2) to obtain the viscosity of water inside the nanotubes. The viscosity values are listed in Table 2 and plotted in Fig. 6a as a function of temperature. Table S1 of ESI,† presents the comparison of simulated viscosities of water using GK, CSE, and JCSE approaches. The viscosities of water inside hydrophobic CNTs are also plotted in the same figure to facilitate the comparison between the two. The most striking result in Fig. 6a is that for a given temperature, water in a superhydrophobic CNT is less viscous than that in the hydrophobic CNT of the same diameter. Similar to diffusivity, the maximum deviation in viscosity is observed for CNT(10,10). For example, at 300 K, the viscosity of water inside superhydrophobic CNT(10,10) is ~3 times less than that in hydrophobic CNT(10,10), as shown in Fig. 6b. This difference increases with the decrease in temperature, such that at 230 K, the viscosity of water in superhydrophobic CNTs is ~20 times less than that in hydrophobic CNTs. Interestingly, the viscosity of water inside superhydrophobic CNTs is lower than that in bulk water, as shown in Fig. 6c. The difference between bulk water and water in superhydrophobic CNTs is significantly large in the wider CNTs. As the temperature decreases, the difference between the viscosities of bulk water and superhydrophobic CNTs increases. At 230 K, water inside superhydrophobic CNT(10,10) is almost two times less viscous than bulk water, while water inside CNT (20,20) is ~4 times less viscous than bulk water. This significantly less viscosity of water inside superhydrophobic CNTs puts forward a much wider range of applications in different areas such as fast desalination of water and water filtration.[8–11] We expect a further reduction in viscosity with the increase in pore width to a minimum value. However, this is out of the scope of this current paper.

3.4. Hydrogen-bonding analyses

Let us now shift our focus to the influence of confinement on the H-bond strength between water molecules and draw a connection with the observed increase in viscosity. The specific geometric conditions[24,89–94] for a hydrogen bond are as follows: the distance between the oxygen atom of the donor molecule (denoted as D) and the oxygen atom of the acceptor molecule (denoted as A) should be less than 3.5 Å and the angle formed

Table 2 The jump frequency ν_{Jump_z}, average square jump length $\lambda_{\mathrm{Jump}_z}{}^2$, the jump-diffusion coefficient D_{Jump_z}, the residual diffusion coefficient D_{Res_z}, percentage contribution of jump-diffusion $\chi_{\mathrm{Jump}(\%)}$, and simulated viscosity values at different temperatures for bulk water and water inside superhydrophobic CNTs. (The viscosity of water is obtained through JCSE approach for water inside CNTs and *via* the GK relation for bulk water)

T (K)	ν_{Jump_z} (ns^{-1})	$\lambda_{\mathrm{Jump}_z}{}^2$ (Å^2)	$D_{\mathrm{Jump}_z}/10^{-5}$ ($\mathrm{cm}^2\,\mathrm{s}^{-1}$)	$D_{\mathrm{Res}_z}/10^{-5}$ ($\mathrm{cm}^2\,\mathrm{s}^{-1}$)	χ_{Jump} (%)	η (cP)
Bulk water						
300	1.88	44.04	0.063	2.040	2.98	0.80
290	2.42	31.90	0.069	1.490	4.40	0.95
280	3.04	23.67	0.074	1.130	6.15	1.35
270	3.01	18.70	0.065	0.847	7.15	1.88
260	2.03	20.61	0.046	0.465	9.05	2.90
250	1.80	18.72	0.039	0.284	12.13	5.04
240	0.95	19.61	0.021	0.144	12.85	9.32
230	0.60	18.37	0.013	0.059	18.13	29.26
CNT(10,10)						
300	1.28	14.2	0.046	1.610	2.76	1.26
290	0.85	22.06	0.047	1.310	3.45	1.42
280	1.16	18.62	0.054	1.010	5.08	1.52
270	1.33	15.64	0.052	0.758	6.44	2.40
260	1.43	13.4	0.048	0.548	8.06	3.04
250	0.86	15.24	0.033	0.375	8.00	4.42
240	0.91	12.62	0.029	0.236	10.81	8.11
230	0.72	12.08	0.022	0.135	13.91	18.40
CNT(15,15)						
300	0.30	15.36	0.011	2.090	0.54	0.88
290	1.12	12.28	0.034	1.750	1.92	1.02
280	1.36	12.7	0.043	1.370	3.05	1.07
270	1.33	13.14	0.044	1.050	4.00	1.66
260	1.91	11.1	0.053	0.759	6.53	2.10
250	1.90	10.12	0.048	0.525	8.37	3.03
240	1.77	8.82	0.039	0.338	10.34	5.44
230	1.04	9.4	0.024	0.208	10.52	11.60
CNT(20,20)						
300	1.28	13.62	0.044	2.620	1.10	0.73
290	1.75	12.36	0.054	2.080	1.16	0.84
280	2.10	11.26	0.059	1.620	1.26	0.89
270	2.73	10.46	0.071	1.210	1.50	1.40
260	2.13	11.67	0.062	0.887	2.41	1.76
250	1.35	13.19	0.044	0.602	4.03	2.58
240	1.54	10.49	0.040	0.388	4.25	4.64
230	1.58	8.52	0.034	0.224	4.72	10.50

among the hydrogen atom of the H-bond donor water, the oxygen atom of the donor molecule, and the oxygen atom of the acceptor molecule (denoted as $H_DO_DO_A$) should be less than 30°. The number of H-bonds per water molecule in bulk water at room temperature is presented in Table S3 of the ESI,† and compared with the values reported in the literature. In Fig. 7a, we plotted the temperature dependence of a average number of H-bonds per water molecule (N_{HB}) for bulk water, water inside superhydrophobic nanotubes, and water inside hydrophobic nanotubes. The profiles for the different systems are nearly parallel to each other, indicating similar linear temperature dependence. As the temperature decreases, the number of hydrogen bonds increases almost linearly. As expected, water confined within the nanotubes has a lower number of hydrogen bonds per water molecule. Specifically, the average number of hydrogen bonds per water molecule in superhydrophobic CNT(10,10) is approximately 10% lower than that in bulk water. For CNT(15,15) and CNT(20,20), the reduction is around 7% and 5%, respectively. When comparing hydrophobic and superhydrophobic nanotubes, it is evident that N_{HB} for superhydrophobic CNT(10,10) is significantly lower than that for hydrophobic CNT(10,10) at all temperatures. However, this difference diminishes as the nanotube diameter increases, reaching almost negligible levels for CNT(20,20). The lower number of hydrogen bonds inside superhydrophobic nanotubes can be attributed to the lower interfacial density of water within these nanotubes compared to hydrophobic ones, as observed in Fig. 2a. The interfacial water molecules are expected to form stronger H-bonds with each other compared to bulk water. Therefore, due to the lower interfacial density in superhydrophobic CNTs, the average number of hydrogen bonds per water molecule is lower than that in hydrophobic CNTs. As the nanotube diameter increases, the dominance of interfacial hydrogen bond structure gradually diminishes.

Although there is a significant reduction in the number of H-bonds per water molecule, the individual H-bonds between water molecules can be stronger when confined inside nanotubes. Our previous study has indeed shown that although the number of H-bonds is less, the individual H-bonds are stronger, and therefore, the total H-bond strength around water confined inside hydrophobic CNTs is higher than that of bulk water. A similar picture is expected for the water confined in superhydrophobic CNTs. To calculate the intermittent H-bond correlation functions C_{HB}, we used the equation shown below $C_{HB}(t)$.[26,36,37,46,49,92,95–102]

$$C_{HB}(t) = \langle h(0)h(t)\rangle/\langle h\rangle \quad (16)$$

We have a function $h(t)$ that takes the value of 1 when two molecules are connected by a hydrogen bond and 0 when that bond is broken. The correlation function $C_{HB}(t)$ describes the probability that a hydrogen bond will remain intact at time t if it was initially intact at time zero, regardless of any potential disruptions during the intervening period. To model the behavior of $C_{HB}(t)$, a tri-exponential function is employed. This function incorporates three exponential terms and can be written as follows:[34,37,50]

$$C_{HB}(t) = a_1\exp(-t/\tau_1) + a_2\exp(-t/\tau_2) + a_3\exp(-t/\tau_3);\ a_1 + a_2 + a_3 = 1. \quad (17)$$

The average H-bond lifetime can be calculated using the following equation: $\tau_{HB} = a_1\tau_1 + a_2\tau_2 + a_3\tau_3$. Fig. S7 of the ESI,† presents $C_{HB}(t)$ as a function of time for all the systems and temperatures. The fitting parameters are listed in Table S2 of the ESI.† We plotted τ_{HB} as a function of temperature in Fig. 7b for four systems including bulk water. The data for hydrophobic systems are also shown in the same figure. Although τ_{HB} for superhydrophobic CNT(10,10) is significantly lower than that for hydrophobic CNT(10,10), the former is still higher than that of bulk water. It suggests that although water–water H-bonds inside the above-mentioned superhydrophobic nanotube are weaker than those inside the hydrophobic nanotube, bulk water H-bonds are still weaker. The free energy of activation for breaking an H-bond can be calculated using the Eyring equation.[102] We determine the Gibbs free energy of activation

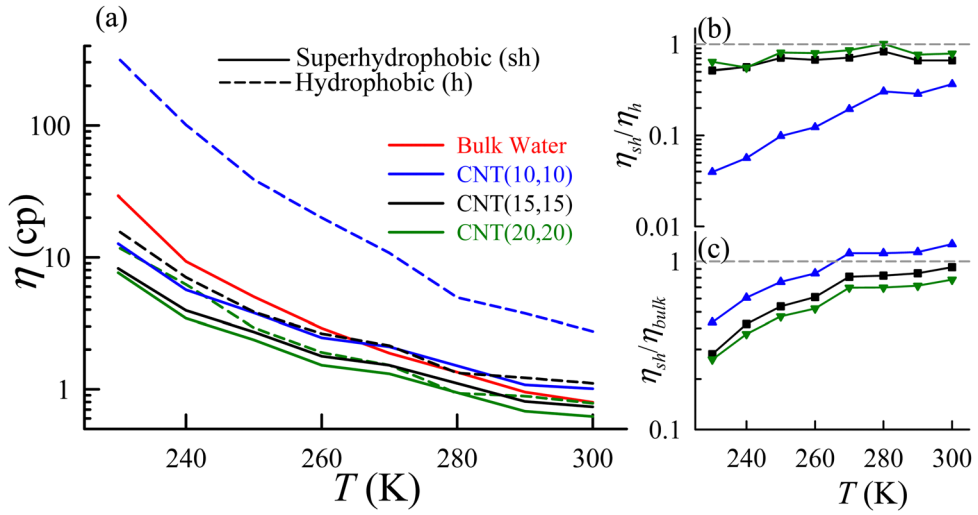

Fig. 6 (a) Temperature-dependent viscosity of water, estimated using the JCSE approach, inside the superhydrophobic (solid line) and the hydrophobic (dashed line) CNTs, and bulk water. (b) Ratio of viscosities of water inside superhydrophobic (sh) and hydrophobic (h) nanotubes as a function of temperature. (c) Temperature-dependent ratio of viscosities of water inside superhydrophobic and bulk water. The data for hydrophobic CNTs and bulk water are taken from our previous work.[34]

ΔG^* for breaking a H-bond at temperature T using the following equation,[34,50]

$$\Delta G^* = k_B T \ln\left(\frac{k_B T}{h}\tau_{HB}\right) \quad (18)$$

In eqn (18), h is the Planck's constant and k_B is the Boltzmann constant. $\Delta G^*_{tot} = N_{HB} \times \Delta G^*$ is the total Gibbs free energy of activation ΔG^*_{tot} to break all H-bonds around a water molecule. Therefore, ΔG^*_{tot} is the total free energy of water molecules bonded to the neighbours. Table S2 of the ESI,† presents ΔG^* and ΔG^*_{tot} for different systems, where we presented the results for superhydrophobic CNTs and bulk water. We plotted ΔG^*_{tot} as a function of temperature for different systems in Fig. 7c. The significant weakening of water–water hydrogen bonds in superhydrophobic CNTs, compared to that in hydrophobic CNTs, can be explained by the lower radial density of water in the interfacial region of the superhydrophobic nanotubes. It is known that water–water hydrogen bonds near the hydrophobic surface are stronger than those in the bulk-like core region due to the presence of tangential H-bonds.[103–106] Consequently, due to the breaking and weakening of hydrogen bonds, water molecules diffuse more rapidly inside superhydrophobic CNTs and experience a lower viscosity than those in hydrophobic nanotubes. The difference between hydrophobic and superhydrophobic cases is most pronounced for CNT(10,10), but it diminishes considerably for CNT(20,20) and becomes nearly negligible.

4. Conclusion

In this study, we employed the jump-corrected confined Stokes–Einstein (JCSE) approach to determine the viscosity of water within a superhydrophobic nanotube over a temperature range of 230 to 300 K. By taking into account both the correction for system size and the correction related to translational jump-induced Stokes–Einstein breakdown, we ensured accurate estimations of the viscosity. We considered three different types of nanotubes: CNT(10,10), CNT(15,15), and CNT(20,20). We compared the fluidity of water inside superhydrophobic and hydrophobic nanotubes with that of bulk water. Our findings revealed that water exhibited a significantly lower viscosity and higher diffusion inside the superhydrophobic CNT(10,10) than inside the hydrophobic CNT(10,10). This difference became more pronounced as the temperature decreased. At 300 K, water in the superhydrophobic CNT(10,10) was approximately three times less viscous than water in the hydrophobic CNT(10,10). However, at 230 K, the former was about twenty times less viscous than the latter. Furthermore, the viscosity of water inside the superhydrophobic nanotube was lower than that of bulk water. While water in the hydrophobic CNT(10,10) exhibited a viscosity roughly three times higher than that of bulk water at 300 K, the difference between bulk water and water in the superhydrophobic CNT(10,10) was much smaller. Interestingly, water inside the wider superhydrophobic CNT(15,15) and CNT(20,20) displayed a lower viscosity and higher diffusion than those of bulk water. As the temperature decreased, the difference in viscosities between bulk water and the superhydrophobic CNTs increased. At 230 K, water inside the superhydrophobic CNT(10,10) was approximately two times less viscous than bulk water, while water inside the CNT(20,20) was about four times less viscous than bulk water.

To investigate the reason behind the lower viscosity of water in superhydrophobic CNTs compared to hydrophobic CNTs, we conducted analyses of hydrogen bonding. We examined the average number of hydrogen bonds per water molecule, the lifetime of hydrogen bonds, and the free energy required

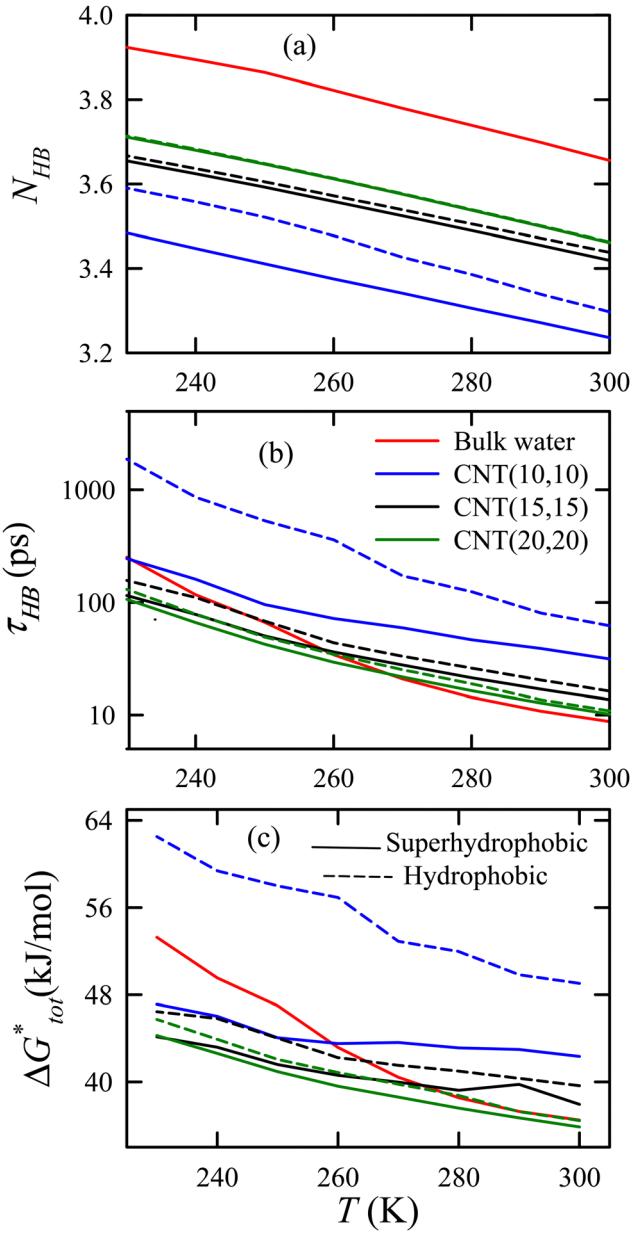

Fig. 7 Comparison between the bulk water, and water inside the hydrophobic and superhydrophobic CNTs: (a) total number of H-bonds per water molecule N_{HB}, (b) water–water H-bond lifetime τ_{HB}, and (c) total free-energy of activation for breaking of all H-bonds around a water molecule ΔG^*_{tot} for all temperatures. The data for hydrophobic CNTs and bulk water are taken from our previous work.[34]

to break all hydrogen bonds surrounding a water molecule. The reduced viscosity of water in superhydrophobic CNTs was attributed to weaker hydrogen bonding interactions between water molecules, resulting from the lower density of water in the interfacial region, where stronger water–water hydrogen bonding occurs. Therefore, the more dispersed density of water inside superhydrophobic CNTs plays a major role in reducing the viscosity of water. This conclusion carries significant importance and was derived from our study. Finally, one should note that the results presented here can be changed quantitatively depending on the chemical nature and roughness of the superhydrophobic surface.

Conflicts of interest

The authors declare no competing financial interest.

Acknowledgements

We thank Mr Tonmoy Sarma for his assistance in calculating the contact angle of water droplet on graphene surface. We acknowledge the Science and Engineering Research Board (SERB) MATRICS for funding (Project No. MTR/2022/000151) and IIT Patna for the computational facility G. R. K. acknowledges IIT Patna for his research fellowship. This paper is dedicated to Prof. Amalendu Chandra (IIT Kanpur) on the occasion of his 60th birthday and for his immense contribution in the field of theoretical physical chemistry.

References

1 L. Cao, I.-C. Chen, C. Chen, D. B. Shinde, X. Liu, Z. Li, Z. Zhou, Y. Zhang, Y. Han and Z. Lai, *J. Am. Chem. Soc.*, 2022, **144**, 12400–12409.
2 C. Fang, D. Huang and J. Su, *J. Phys. Chem. Lett.*, 2020, **11**, 940–944.
3 Y. Qian, D. Liu, G. Yang, L. Wang, Y. Liu, C. Chen, X. Wang and W. Lei, *J. Am. Chem. Soc.*, 2022, **144**, 13764–13772.
4 Z. Zhang, P. Bhauriyal, H. Sahabudeen, Z. Wang, X. Liu, M. Hambsch, S. C. Mannsfeld, R. Dong, T. Heine and X. Feng, *Nat. Commun.*, 2022, **13**, 3935.
5 M. I. Sajid, U. Jamshaid, T. Jamshaid, N. Zafar, H. Fessi and A. Elaissari, *Int. J. Pharm.*, 2016, **501**, 278–299.
6 S. Kar, R. Bindal and P. Tewari, *Nano Today*, 2012, **7**, 385–389.
7 B. Corry, *Energy Environ. Sci.*, 2011, **4**, 751–759.
8 B. Corry, *J. Phys. Chem. B*, 2008, **112**, 1427–1434.
9 Y. Hong, J. Zhang, C. Zhu, X. C. Zeng and J. S. Francisco, *J. Mater. Chem. A*, 2019, **7**, 3583–3591.
10 R. Das, M. E. Ali, S. B. Abd Hamid, S. Ramakrishna and Z. Z. Chowdhury, *Desalination*, 2014, **336**, 97–109.
11 K. Gethard, O. Sae-Khow and S. Mitra, *ACS Appl. Mater. Interfaces*, 2011, **3**, 110–114.
12 M. Sathiya, A. Prakash, K. Ramesha, J. M. Tarascon and A. K. Shukla, *J. Am. Chem. Soc.*, 2011, **133**, 16291–16299.
13 S. Mondal and B. Bagchi, *J. Chem. Phys.*, 2020, **152**, 224707.
14 S. Kumar and B. Bagchi, *J. Chem. Phys.*, 2022, **156**, 224501.
15 A. Chatzichristos and J. Hassan, *Nanomaterials*, 2022, **12**, 174.
16 A. Chatzichristos and J. Hassan, *Nanomaterials*, 2022, **12**(1), 174.
17 X. Qin, Q. Yuan, Y. Zhao, S. Xie and Z. Liu, *Nano Lett.*, 2011, **11**, 2173–2177.
18 M. Majumder, N. Chopra, R. Andrews and B. J. Hinds, *Nature*, 2005, **438**, 44.

19 M. Majumder, N. Chopra, R. Andrews and B. Hinds, *Nature*, 2005, **438**, 930.
20 J. K. Holt, H. G. Park, Y. Wang, M. Stadermann, A. B. Artyukhin, C. P. Grigoropoulos, A. Noy and O. Bakajin, *Science*, 2006, **312**, 1034–1037.
21 E. Secchi, S. Marbach, A. Niguès, D. Stein, A. Siria and L. Bocquet, *Nature*, 2016, **537**, 210–213.
22 A. Zaragoza, M. A. González, L. Joly, I. López-Montero, M. Canales, A. Benavides and C. Valeriani, *Phys. Chem. Chem. Phys.*, 2019, **21**, 13653–13667.
23 S. Mondal and B. Bagchi, *J. Phys. Chem. Lett.*, 2019, **10**, 6287–6292.
24 B. H. Mendonça, P. Ternes, E. Salcedo, A. B. de Oliveira and M. C. Barbosa, *J. Chem. Phys.*, 2020, **153**, 024708.
25 G. Cicero, J. C. Grossman, E. Schwegler, F. Gygi and G. Galli, *J. Am. Chem. Soc.*, 2008, **130**, 1871–1878.
26 G. Hummer, J. C. Rasaiah and J. P. Noworyta, *Nature*, 2001, **414**, 188–190.
27 H. Ye, H. Zhang, Y. Zheng and Z. Zhang, *Microfluid. Nanofluid.*, 2011, **10**, 1359–1364.
28 B. H. Mendonça, E. E. de Moraes, R. J. Batista, A. B. de Oliveira, M. C. Barbosa and H. Chacham, *J. Phys. Chem. C*, 2023, **127**, 9769–9778.
29 N. Galamba, *J. Phys.: Condens. Matter*, 2016, **29**, 015101.
30 T. Chen, B. Smit and A. T. Bell, *J. Chem. Phys.*, 2009, **131**, 246101.
31 P. J. Daivis and D. J. Evans, *J. Chem. Phys.*, 1994, **100**, 541–547.
32 M. Mondello and G. S. Grest, *J. Chem. Phys.*, 1997, **106**, 9327–9336.
33 M. H. Köhler, J. R. Bordin, L. B. da Silva and M. C. Barbosa, *Phys. Chem. Chem. Phys.*, 2017, **19**, 12921–12927.
34 G. R. Khan and S. Daschakraborty, *J. Phys. Chem. C*, 2023, **127**, 7027–7035.
35 P. Simonnin, B. T. Noetinger, C. Nieto-Draghi, V. Marry and B. Rotenberg, *J. Chem. Theory Comput.*, 2017, **13**, 2881–2889.
36 V. Dubey, S. Erimban, S. Indra and S. Daschakraborty, *J. Phys. Chem. B*, 2019, **123**, 10089–10099.
37 S. Dueby, V. Dubey and S. Daschakraborty, *J. Phys. Chem. B*, 2019, **123**, 7178–7189.
38 A. Dehaoui, B. Issenmann and F. Caupin, *Proc. Natl. Acad. Sci. U. S. A.*, 2015, **112**, 12020–12025.
39 P. Kumar, *Proc. Natl. Acad. Sci. U. S. A.*, 2006, **103**, 12955–12956.
40 S.-H. Chen, F. Mallamace, C.-Y. Mou, M. Broccio, C. Corsaro, A. Faraone and L. Liu, *Proc. Natl. Acad. Sci. U. S. A.*, 2006, **103**, 12974–12978.
41 L. P. Singh, B. Issenmann and F. Caupin, *Proc. Natl. Acad. Sci. U. S. A.*, 2017, **114**, 4312–4317.
42 J. Bartak, *Int. J. Multiphase Flow*, 1990, **16**, 789–798.
43 S. Banerjee, P. K. Ghorai, D. Maji and R. Biswas, *J. Phys. Chem. B*, 2022, **126**, 10146–10155.
44 C. Corsaro, E. Fazio and D. Mallamace, *J. Chem. Phys.*, 2019, **150**, 234506.
45 S. Dueby, V. Dubey, S. Indra and S. Daschakraborty, *Phys. Chem. Chem. Phys.*, 2022, **24**, 18738–18750.
46 V. Dubey and S. Daschakraborty, *J. Phys. Chem. B*, 2020, **124**, 10398–10408.
47 S. Erimban and S. Daschakraborty, *J. Phys. Chem. B*, 2023, **127**(22), 4939–4951.
48 S. Dueby and S. Daschakraborty, *Chem. Phys. Lett.*, 2022, **806**, 140059.
49 V. Dubey, S. Dueby and S. Daschakraborty, *Phys. Chem. Chem. Phys.*, 2021, **23**, 19964–19986.
50 V. Dubey and S. Daschakraborty, *J. Phys. Chem. B*, 2022, **126**, 2430–2440.
51 A. Kumar and S. Daschakraborty, *Phys. Chem. Chem. Phys.*, 2023, **25**, 31431–31443.
52 Y. Li, Z. Li, F. Aydin, J. Quan, X. Chen, Y.-C. Yao, C. Zhan, Y. Chen, T. A. Pham and A. Noy, *Sci. Adv.*, 2020, **6**, eaba9966.
53 J. P. Rothstein, *Annu. Rev. Fluid Mech.*, 2010, **42**, 89–109.
54 K.-Y. Law, *Journal*, 2014, **5**, 686–688.
55 W. Barthlott and C. Neinhuis, *Planta*, 1997, **202**, 1–8.
56 C. Neinhuis and W. Barthlott, *Ann. Bot.*, 1997, **79**, 667–677.
57 D. Wang, Q. Sun, M. J. Hokkanen, C. Zhang, F.-Y. Lin, Q. Liu, S.-P. Zhu, T. Zhou, Q. Chang and B. He, *Nature*, 2020, **582**, 55–59.
58 S. Parvate, P. Dixit and S. Chattopadhyay, *J. Phys. Chem. B*, 2020, **124**, 1323–1360.
59 T. Lv, Z. Cheng, D. Zhang, E. Zhang, Q. Zhao, Y. Liu and L. Jiang, *ACS Nano*, 2016, **10**, 9379–9386.
60 A. K. Kota, J. M. Mabry and A. Tuteja, *Surface Innovations*, 2013, **1**, 71–83.
61 S. Nishimoto and B. Bhushan, *RSC Adv.*, 2013, **3**, 671–690.
62 E. Celia, T. Darmanin, E. T. de Givenchy, S. Amigoni and F. Guittard, *J. Colloid Interface Sci.*, 2013, **402**, 1–18.
63 J. Drelich and A. Marmur, *Surface Innovations*, 2014, **2**, 211–227.
64 S. He, J. Wei, H. Wang, D. Sun, Z. Yao, C. Fu, R. Xu, Y. Jia, H. Zhu and K. Wang, *Nanoscale Res. Lett.*, 2013, **8**, 1–6.
65 V. S. Saji, *Nanotechnol. Rev.*, 2021, **10**, 518–571.
66 A. Tuteja, W. Choi, M. Ma, J. M. Mabry, S. A. Mazzella, G. C. Rutledge, G. H. McKinley and R. E. Cohen, *Science*, 2007, **318**, 1618–1622.
67 X. Chen, J. A. Weibel and S. V. Garimella, *Sci. Rep.*, 2015, **5**, 17110.
68 J. Barman, S. K. Majumder, P. K. Roy and K. Khare, *RSC Adv.*, 2018, **8**, 13253–13258.
69 A. Grigoryev, I. Tokarev, K. G. Kornev, I. Luzinov and S. Minko, *J. Am. Chem. Soc.*, 2012, **134**, 12916–12919.
70 X. Tian, V. Jokinen, J. Li, J. Sainio and R. H. Ras, *Adv. Mater.*, 2016, **28**, 10652–10658.
71 M. H. Köhler and L. B. da Silva, *Chem. Phys. Lett.*, 2016, **645**, 38–41.
72 Y. Liu, Q. Wang, T. Wu and L. Zhang, *J. Chem. Phys.*, 2005, **123**, 234701.
73 H. Zhang, H. Ye, Y. Zheng and Z. Zhang, *Microfluid. Nanofluid.*, 2011, **10**, 403–414.
74 W. L. Jorgensen and J. Tirado-Rives, *J. Am. Chem. Soc.*, 1988, **110**, 1657–1666.

75 I. Zeron, J. Abascal and C. Vega, *J. Chem. Phys.*, 2019, **151**, 134504.
76 I. Moskowitz, M. A. Snyder and J. Mittal, *J. Chem. Phys.*, 2014, **141**, 18C532.
77 A. Waghe, J. C. Rasaiah and G. Hummer, *J. Chem. Phys.*, 2002, **117**, 10789–10795.
78 M. J. De Ruijter, T. Blake and J. De Coninck, *Langmuir*, 1999, **15**, 7836–7847.
79 S. Nosé, *J. Chem. Phys.*, 1984, **81**, 511–519.
80 W. G. Hoover, *Phys. Rev. A*, 1985, **31**, 1695.
81 A. Rahman, *Phys. Rev.*, 1964, **136**, A405.
82 V. Dubey, N. Kumar and S. Daschakraborty, *J. Phys. Chem. B*, 2018, **122**, 7569–7583.
83 V. Dubey and S. Daschakraborty, *Phys. Chem. Chem. Phys.*, 2019, **21**, 800–812.
84 G. E. Uhlenbeck and L. S. Ornstein, *Phys. Rev.*, 1930, **36**, 823.
85 M. C. Wang and G. E. Uhlenbeck, *Rev. Mod. Phys.*, 1945, **17**, 323.
86 D. Freedman, *Brownian motion and diffusion*, Springer Science & Business Media, 2012.
87 V. Dubey, S. Dueby, S. Erimban and S. Daschakraborty, *J. Indian Chem. Soc.*, 2019, **96**, 741–751.
88 V. Dubey, A. Maiti and S. Daschakraborty, *Chem. Phys. Lett.*, 2020, **755**, 137802.
89 D. Chakraborty and A. Chandra, *J. Chem. Phys.*, 2011, **135**, 114510.
90 G. Gilli and P. Gilli, *The nature of the hydrogen bond: outline of a comprehensive hydrogen bond theory*, Oxford university press, 2009.
91 D. Laage and J. T. Hynes, *Science*, 2006, **311**, 832–835.
92 A. Luzar and D. Chandler, *Phys. Rev. Lett.*, 1996, **76**, 928.
93 J. Stenger, D. Madsen, P. Hamm, E. T. Nibbering and T. Elsaesser, *J. Phys. Chem. A*, 2002, **106**, 2341–2350.
94 D. Laage and J. T. Hynes, *J. Phys. Chem. B*, 2008, **112**, 14230–14242.
95 A. Chandra, *Phys. Rev. Lett.*, 2000, **85**, 768.
96 S. Chowdhuri and A. Chandra, *Phys. Rev. E*, 2002, **66**, 041203.
97 B. Bagchi, *Chem. Rev.*, 2005, **105**, 3197–3219.
98 N. Rawat and P. Biswas, *J. Phys. Chem. B*, 2014, **118**, 3018–3025.
99 S. Indra and R. Biswas, *Mol. Simul.*, 2015, **41**, 471–482.
100 A. Luzar and D. Chandler, *Nature*, 1996, **379**, 55–57.
101 A. Luzar, *J. Chem. Phys.*, 2000, **113**, 10663–10675.
102 S. Balasubramanian, S. Pal and B. Bagchi, *Phys. Rev. Lett.*, 2002, **89**, 115505.
103 D. Laage, T. Elsaesser and J. T. Hynes, *Chem. Rev.*, 2017, **117**, 10694–10725.
104 G. Stirnemann, P. J. Rossky, J. T. Hynes and D. Laage, *Faraday Discuss.*, 2010, **146**, 263–281.
105 D. Laage, G. Stirnemann and J. T. Hynes, *Sci. China Phys., Mech. Astronomy*, 2010, **53**, 1068–1072.
106 S. K. Pal, J. Peon, B. Bagchi and A. H. Zewail, *J. Phys. Chem. B*, 2002, **106**, 12376–12395.

